ISEV

RESEARCH ARTICLE

Untouched isolation enables targeted functional analysis of tumour-cell-derived extracellular vesicles from tumour tissues

Zi-Li Yu[1,2] | Xing-Chi Liu[1] | Min Wu[1] | Shan Shi[1] | Qiu-Yun Fu[1] | Jun Jia[1,2] | Gang Chen[1,2,3]

[1]The State Key Laboratory Breeding Base of Basic Science of Stomatology (Hubei-MOST) & Key Laboratory of Oral Biomedicine Ministry of Education, School and Hospital of Stomatology, Wuhan University, Wuhan 430079, China

[2]Department of Oral and Maxillofacial Surgery, School and Hospital of Stomatology, Wuhan University, Wuhan 430079, China

[3]Frontier Science Center for Immunology and Metabolism, Wuhan University, Wuhan 430071, China

Correspondence
Gang Chen and Jun Jia, The State Key Laboratory Breeding Base of Basic Science of Stomatology (Hubei-MOST) & Key Laboratory of Oral Biomedicine Ministry of Education, School and Hospital of Stomatology, Wuhan University, Wuhan 430079, China.
Email: geraldchan@whu.edu.cn and junjia@whu.edu.cn

Zi-Li Yu and Xing-Chi Liu contributed equally to this work.

Abstract
To accurately identify the functions of tumour-cell-derived extracellular vesicles (T-EVs), EVs directly isolated from tumour tissues are much preferred over those derived from in vitro cultured tumour cell lines. However, the functional analysis of T-EVs has still been severely limited by the difficulty in selective isolation of T-EVs from tissue-derived heterogeneous EVs, which also contain non-tumour cell-derived EVs. We here establish an untouched isolation strategy that specifically collects natural T-EVs from tumour tissues by removing non-tumour-cell-derived EVs. Different from traditional immunomagnetic separation, our isolation materials are directly bound to undesired non-tumour-cell-derived EVs, preserving the natural properties of T-EVs. Using this strategy, we reveal the distinct performances of tissue-derived T-EVs in organotropism to lymph nodes, immunosuppression and angiogenesis. The present work, which takes an extraordinary step forward in the isolation of EV subpopulation from tumour tissues, would dramatically accelerate the investigation of EV heterogeneity.

KEYWORDS
extracellular vesicles, functional analysis, isolation, subpopulation, untouched

1 | INTRODUCTION

Extracellular vesicles (EVs) are naturally occurring nano-sized membrane-bound vesicles released by nearly all cell types and diffusely exist in all body fluids and tissues (Kalluri & Lebleu, 2020; Möller & Lobb, 2020). The molecular profiles of EVs are

inherited from their parent cells and can partially represent the status of donor cells (Xu et al., 2018). As important intercellular communication vectors, EVs convey bioactive molecules between cells, playing significant roles in many important biological processes (Raposo & Stoorvogel, 2013; Tkach & Théry, 2016). Studies including our own have reported that tumour-cell-derived EVs (T-EVs) may play critical roles in the development of tumour, but the underlying mechanisms are still little understood (Chen et al., 2018; Ren et al., 2016a, 2016b; Zhong et al., 2019). The EVs, being employed to reveal the accurate mechanisms by which EVs affect tumour development, should reflect unlimitedly the real status of T-EVs. Currently, EVs used in the majority of previous studies were those collected from in vitro cultured tumour cell lines, which were assumed to be the parent cells of T-EVs (Morrissey et al., 2021). Obviously, after years of in vitro culture, tumour cell lines, which originated from a single individual at a specific time during tumour development, cannot reflect the dynamic state of tumours. Moreover, the in vitro cultured tumour cell lines lose their interactions with other cell types or stimulators (such as cytokines) that normally coexist in the tumour microenvironment. Due to the distinct growth environment of parent cells, those alleged T-EVs produced in vitro may have distinct cargo compositions and performances in comparison to T-EVs secreted in tumour microenvironment (Crescitelli et al., 2021; Domcke et al., 2013). Therefore, to accurately identify their functions during tumour development, T-EVs directly isolated from cancer patients are much more preferred. Actually, T-EVs diffusely exist in circulation and tumour tissues. Because T-EVs are diluted in bloodstream to a large extent, EVs in circulation are completely dominated by non-tumour-cell-produced EVs, hindering successful isolation and identification of the functions of T-EVs. More importantly, the original properties of T-EVs in the circulation can also be influenced after interaction with proteins or other admixtures in serum. Therefore, the fresh T-EVs in the tumour tissues, which could more accurately reflect the pathophysiological characteristics and behaviours of real T-EVs, may be the better source for accurate functional analysis.

To identify their characteristics and biological functions, the first and essential step is to separate T-EVs from tumour tissues. However, conventional methods, including ultracentrifugation, size-exclusion chromatography (SEC) and precipitation, fail to selectively separate the subpopulation of T-EVs form heterogeneous EVs. In the past few years, microfluidic-based technologies have emerged to play an essential role in the isolation, detection and analysis of EV subpopulations (Casadei et al., 2021; Liu et al., 2019, 2018). Currently, microfluidic-based separation techniques mostly fall into two categories: (i) immunoaffinity-based isolation utilizing antibodies or aptamers, (ii) label-free separation based on the electrical and physical prosperities of EVs by combining microfluidics with acoustic waves and dielectric electrophoresis (Wang et al., 2021). Among them, immunoaffinity-based separation, also known as 'positive isolation strategy', is used in selective separation of EVs carrying indicated surface markers (Jeppesen et al., 2019; Reátegui et al., 2018; Sharma et al., 2018). However, it should be noted that a number of drawbacks are associated (Shao et al., 2018). First, the surface marker-based isolation strategy is only available for the positively marked EV subtypes but not the negative ones. Second, EVs trapped on the magnetic beads or narrow channels of chips, which are usually significantly larger and heavier than natural ones, losing their natural physical properties and biological function (Ramirez et al., 2018). Third, even if those restricted EVs regain their liberty by breaking the connection between beads and antibodies, surface markers of EVs are still masked by antibodies (Cai et al., 2018). Moreover, the reagents used to break the cross-links will also compromise the structure of surface proteins on EVs. Previous studies, including those from our laboratory, have revealed that blockage of surface markers (e.g. integrin and PD-L1) will significantly change their distribution pattern and severely impair their performances in vivo (Chen et al., 2018; Hoshino et al., 2015). In this regard, the marker-blocked EVs cannot represent natural intact counterparts. The label-free isolation of EVs on microfluidic chips without the use of antibody or aptamer, is promising for isolating EV subpopulations. At current stage, however, this strategy is more applicable to separate EV subpopulations with different size, electrical characteristics and deformability, but not the EVs with indicated surface markers. Therefore, it is highly desirable to develop a biofriendly strategy to purify T-EVs from tumour tissues without unfavourable effects on their original properties. Such a strategy would also dramatically promote the investigation of true EV functions and identification of EV-based biomarker.

Inspired by our years of experience in the isolation of EVs (Chen et al., 2015; Yu et al., 2021; Zhang et al., 2017), we here developed an untouched isolation strategy to selectively purify T-EVs form tumour tissues, which was realized by removing non-tumour-cell-derived EVs (Figure 1). Different from the positive isolation strategy, the isolating materials in this strategy were directly binding to the undesired non-tumour-cell-derived EVs rather than T-EVs. Thus, this strategy was also termed as 'negative isolation strategy'. Our results demonstrated that the natural properties of T-EVs, including the morphology, size, cargo composition and capability to be internalized into target cells, were maximally preserved by such an untouched isolation strategy. We revealed that tumour tissue-derived T-EVs can more accurately reflect the pathophysiological characteristics and behaviours of real T-EVs than tumour-cell-line-derived EVs. Using the obtained natural T-EVs, we further revealed their longer circulating lifetime than heterogeneous EVs in vivo. Moreover, our data also suggested that, due to the different profiles of cargos, T-EVs displayed enhanced lymph node-targeting specificity, immunosuppressive and proangiogenic effects than non-tumour-cell-derived EVs. In summary, the present study not only realized the reliable untouched and selective isolation of T-EVs from tumour tissues, and also accurately evaluated their functions. We believe that this work takes an extraordinary step forward in the isolation of EV subpopulation, and will dramatically accelerate the investigation of heterogeneity of EVs.
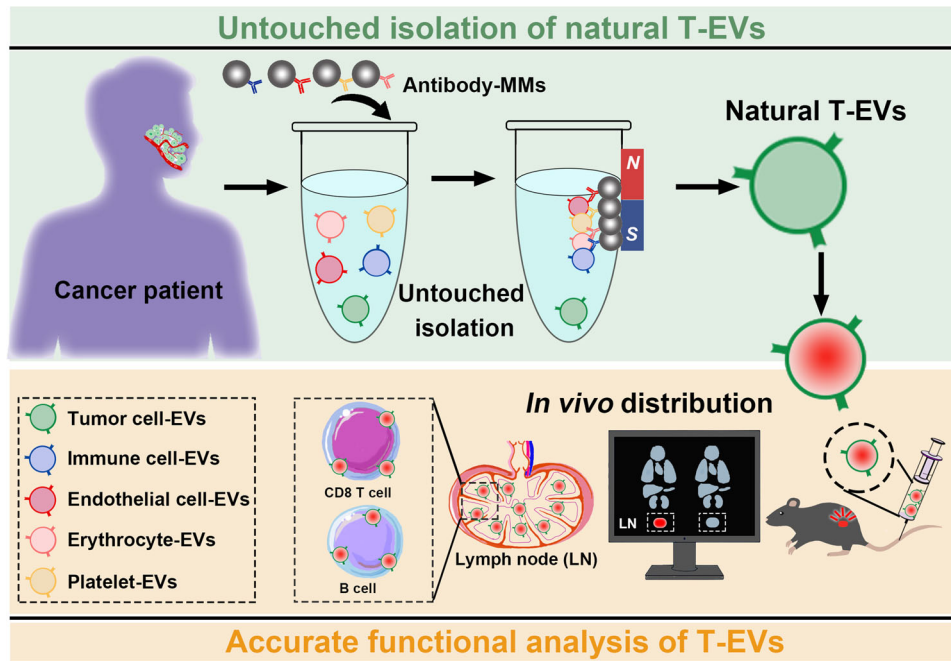
FIGURE 1 Work principle of untouched isolation strategy. Natural tumour-cell-derived extracellular vesicles (T-EVs) in tumour tissues of oral squamous cell carcinoma (OSCC) patients were enriched by removing non-tumour cell-derived EVs

2 | MATERIALS AND METHODS

2.1 | Collection of patient specimen

Tumour tissues and lymph nodes were collected, respectively, from patients with OSCC who underwent biopsy and surgical resection at the Department of Oral and Maxillofacial Surgery, Hospital of Stomatology of Wuhan University, China. Informed consent was obtained from all individuals before sample collection, and ethics permission was granted by the review board of the Ethics Committee of the School and Hospital of Stomatology of Wuhan University. Tumour tissue specimens were delivered instantly to the laboratory by being preserved in plain RPMI-1640 media at 4 °C.

2.2 | Cell culture

Human OSCC cell line (CAL27) and acute lymphoblastic leukaemia Jurkat cell were cultured in DMEM medium and RPMI-1640-Glutamax™ medium (Gibco, CA, USA) both supplemented with 10% foetal bovine serum (FBS), respectively. Human umbilical vein endothelial cells (HUVECs) were cultured in endothelial cell medium supplemented with 20% FBS and 1% endothelial cell growth supplement. All cells were grown at 37 °C in 5% CO_2 humidified incubator.

2.3 | Isolation of EVs from in vitro cultured cells

Cell culture supernatants were collected and EVs were isolated by a standard sequential ultracentrifugation. Apoptotic bodies and cell debris were removed by centrifugation at 3000 g for 20 min at 4 °C twice. Then, the supernatant was centrifuged at 120,000 g for 70 min at 4 °C (Beckman Coulter Optima XE-100, USA; Type 45 Ti rotor) to collect EVs. The pelleted EVs were resuspended in phosphate-buffered saline (PBS).

2.4 | Isolation of EVs from tumour tissues of OSCC patients

Tumour tissues were directly processed for isolating EVs without frozen treatment. Tumour-tissue-derived EVs were isolated according to the protocol reported previously (Crescitelli et al., 2021). In a word, after clearing away residual blood, the collected tumour tissues were sliced into pieces and treated with plain RPMI-1640 media supplemented with collagenase IV (1 mg/ml,

Sigma-Aldrich) and DNase I (0.1 mg/ml, Roche). Cells in tumour tissues were gently dissociated from extracellular matrix by incubating in a shaking incubator at 37 °C for 1 h. The dissociated tissues and single cells were removed by centrifugation at 500 g for 10 min. The supernatant was then transferred to a fresh tube, and sequentially centrifuged at 2000 g for 10 min and 10,000 g for 45 min at 4 °C. EVs were isolated by further centrifugation of the supernatant at 120,000 g for 70 min at 4 °C (Beckman Coulter Optima MAX-XP, MLA-130). The pelleted EVs were resuspended in PBS.

2.5 | Characterization of EVs

The size and concentration of EVs were determined using nanoparticle tracking analysis (NTA, ZetaView, Particle Metrix, Germany). For transmission electron microscopy (TEM) analysis, the isolated EVs (10 $\mu g/\mu l$) were placed on carbon-coated grid for 2 min and washed with PBS twice. After being blotted and air-dried, the samples were stained with 2% uranyl acetate and visualized by using the JEM-1011 transmission electron microscope (Hitachi, Japan). The zeta potential of EVs was determined using a dynamic light scattering (DLS, Zetasizer Nano ZS, Malvern Instruments, UK).

2.6 | Untouched isolation of EVs

After being resuspended in the vial by vibrating for 1 min and rotating for 10 min, the magnetic microparticles (MMs, Invitrogen, Cat# 11417D) were transferred into a tube and washed three times with isolation buffer and then blocked with 5% BSA for 1 h at 4 °C. With MMs being washed three times and resuspended with isolation buffer, the capture antibodies (with 0.2 μg each kind of antibody per 20 μl of MMs) were added into the tubes and incubated with MMs for 1 h at the room temperature. Information about the capture antibodies was included in Supplementary Table 1. The antibody-MMs were washed with isolation buffer three times. Then, the EV samples (25 μg total protein) and 20 μl of MMs were added into the tubes and incubated overnight at 4 °C with a mixer. Subsequently, tubes were placed on the magnet and the supernatant was collected to obtain the purified EVs in the next day.

2.7 | Western blot analysis

Protein concentration was determined by BCA protein assay reagent kit (Beyotime Shanghai, China). After being denatured at 95 °C for 5 min, the whole cell lysates or EVs proteins were separated by 12% SDS-PAGE and transferred onto nitrocellulose membranes. And the membrane was blocked with 5% non-fat dry milk for 1 h at room temperature, and incubated with the corresponding primary antibodies overnight at 4 °C Then, the membrane was followed by incubation with horseradish peroxidase-conjugated secondary antibodies for 1 h at room temperature. The blots on membranes were visualized using the ECL Western Blotting substrate (Advansta, Cat# R-03025-D25) and a Fusion FX device (Sagecreation). Information about the primary antibodies was included in Supplementary Table 1.

2.8 | Flow cytometry of EVs

The whole process of flow cytometry analysis in present study, including the experimental design, sample preparation, assay control and sample staining, was performed according to the standardized framework issued by International Society of Extracellular Vesicles (ISEV) in 2020 (Welsh et al., 2020). The final concentrations of antibodies used for measurement were determined by preliminary experiments. For phenotyping of the EVs isolated from tumour tissues, the EV samples were stained with each kind of antibody separately. Specifically, 1-μl tumour tissue-derived EVs (0.5–1 $\mu g/\mu l$) were diluted with 9-μl PBS supplemented with each of antibody, respectively, for 1 h at room temperature. Then, the EVs were resuspended in 300-μl PBS and analysed with high-resolution flow cytometer (A60, Apogee, UK). For analysing the positivity of a given surface marker on EVs, EVs stained with matched isotype control were used to identify the background non-specific staining and to define the positive gate. Information about the used antibodies was included in Supplementary Table 1.

2.9 | Confocal microscopy imaging

HUVECs were seeded on confocal dishes (3×10^5 cells per well) and grew overnight. Cells were labelled with CFSE and then incubated with WGA-labelled EVs for 15 min. Finally, the images were captured with a confocal microscopy (Andor Revolution XD) and analysed with FV10-ASW4.2 Viewer.

2.10 | Cellular uptake assays

To investigate the cellular internalization of EVs obtained by negative isolation or positive isolation, uptake assays using HUVECs and Jurkat cells as recipient cells were carried out. EVs were stained with CFSE in PBS, and then washed with PBS and pelleted by ultracentrifugation. And the recipient cells were treated with CFSE-labelled EVs (25 μg/ml) for 2 h. Then, the flow cytometry was performed to verify the internalization and data were analysed using FlowJo V10.0 software.

2.11 | In vivo mice study

All animal experiments were approved by the review board of the Ethics Committee of Hospital of Stomatology, Wuhan University. C57BL/6 mice were obtained from Hubei Province Laboratory Animal Public Service Center. Age- and weight-matched healthy C57BL/6 mice were intravenously injected with DiR or CFSE-labelled EVs (100 μl, 1 mg/ml) via tail vein. Peripheral blood samples were harvested at indicated time points after EVs injection. EVs were isolated from circulation by ultracentrifugation. Fluorescence intensity of CFSE-labelled EVs was measured by high-resolution flow cytometry. Twelve hours after injection, mice were euthanized and the major organs were harvested and analysed using Bruker Xtreme BI in vivo fluorescence imaging system. Lymph nodes of mice were collected to harvest single cells. The obtained single cell suspensions were centrifugated at 1500 rpm for 5 min and resuspended in PBS for staining. Information about the primary antibodies was included in Supplementary Table 1. Finally, the samples were analysed by flow cytometry.

2.12 | Tube formation assay

We diluted Matrigel (Corning Matrigel, Cat# 354234) 1:1 with cold endothelial cell growth medium and spread the mixture on 24-well plates. HUVECs (8×10^4) were seeded on Matrigel per well. HUVECs were incubated with EVs for 24 h at 37 °C. After the cells were deformed and adhered to the walls, the capillary tubes were quantified by measuring the total lengths of the completed tubule structure.

2.13 | Flow cytometry of cells from patients' lymph nodes

Single-cell suspensions from patients' lymph nodes were prepared according to standard protocol reported previously (Veerman et al., 2019). The obtained lymph node cells were co-incubated with tumour tissue-derived EVs (25 μg/ml, pre-labelled with CFSE) from the corresponding patients for 24 h. Then, cells were stained with antibodies and detected by the flow cytometry. Information about the primary antibodies was included in Supplementary Table 1.

2.14 | Statistical analysis

All data were analysed using one-way ANOVA or Student's t test at a significance level of $P < 0.05$ in GraphPad Prism 7.0 (GraphPad Software, La Jolla, CA, USA). The results are expressed as the mean $\pm$ SD for three independent experiments.

3 | RESULTS

3.1 | Isolation and characterization of heterogeneous EVs from the tumour tissues

EVs in tumour tissues of OSCC patients were collected with ultracentrifugation (Figure 2a) and verified by TEM and NTA (Figure 2b, c). Tumour tissues consist of tumour cells and non-tumour cells, which were considered as the parental cells of tumour tissue-derived EVs. The relative levels of EVs with indicated surface markers were further quantified by high-resolution flow cytometer (Figure 2d). Results revealed that 36.10% of the EVs carried EpCAM on their surface, which were considered as T-EVs. The largest proportion of tumour-tissue-derived EVs was non-tumour-cell-derived EVs, among which immune cell-derived EVs (I-EVs) showed the highest proportion (52.38%). Other fractions of tumour-tissue-derived EVs were endothelial cell-derived EVs (E-EVs) (5.13%), platelet-derived EVs (P-EVs) (3.37%), red blood cell-derived EVs (R-EVs) (1.54%). The cell sources of tumour-tissue-derived EVs were further determined by western blot analysis. As shown in Figure 2e, markers of tumour cell (EpCAM) and non-tumour cells, such as immune cells (CD45), endothelial cells (CD144), platelet (CD41) and red blood cells (CD235a), were detected in tumour-tissue-derived EVs. The results demonstrated that EVs isolated from tumour tissues were heterogeneous EVs that secreted by both tumour and non-tumour cells.
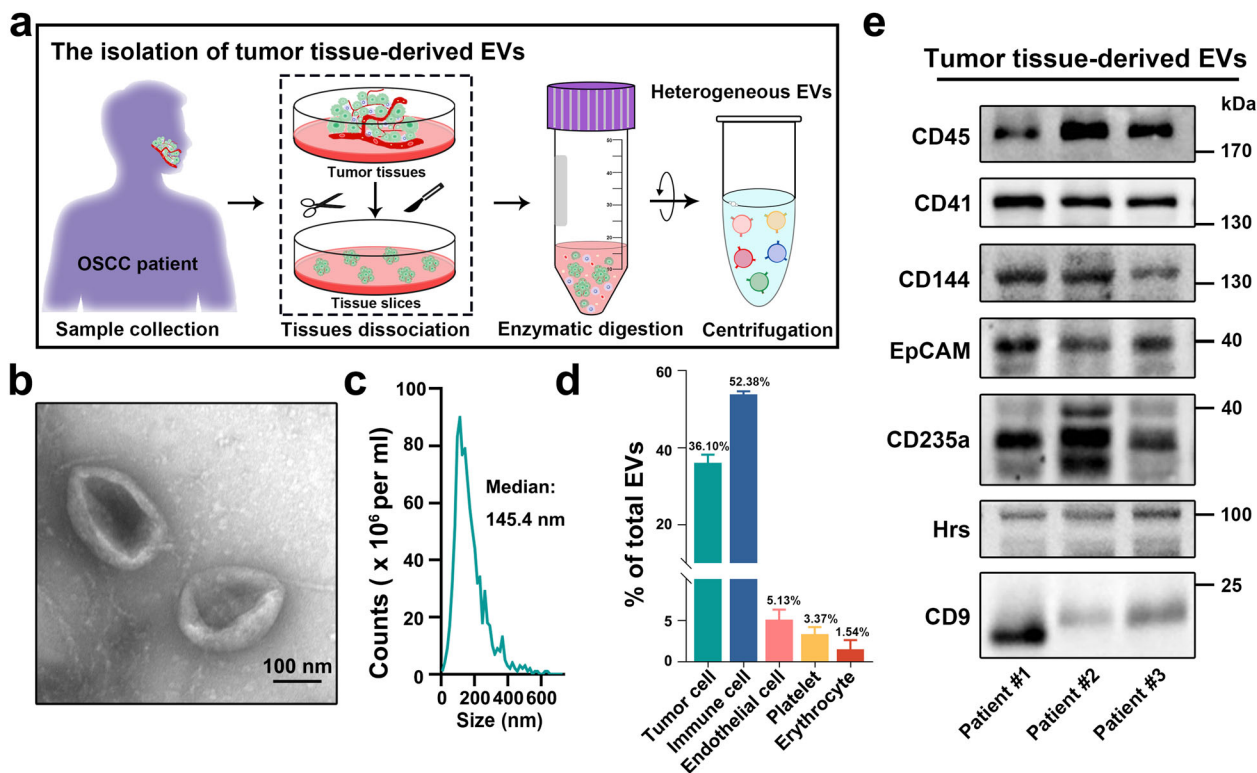
FIGURE 2 Characterization of EVs derived from tumour tissues of oral squamous cell carcinoma (OSCC) patients. (a) Schematic diagram for collection of EVs from tumour tissues of OSCC patients. Characterization of tumour tissue-derived EVs using transmission electron microscopy (b) and nanoparticle tracking analysis (c). (d) Levels of cell source markers on tumour tissue-derived EVs were detected by high-resolution flow cytometry. (e) Western blot analysis of CD45, CD4l, CD144, EpCAM, CD235a, Hrs and CD9 in tumour tissue-derived EVs

3.2 | Design and verification of the untouched and selective enrichment of T-EVs

After determining the cell sources of heterogeneous EVs from tumour tissues, we proposed an untouched strategy for the selective enrichment of T-EVs by removing non-tumour-cell-derived EVs. We first testify the feasibility of the untouched isolation strategy in fabricated heterogeneous EVs (Figure 3a). We purified EVs from culture medium of human OSCC cells (T-EVs), immune cells (I-EVs) and endothelial cells (E-EVs) by differential centrifugation, and verified them by NTA assay (Figure S1a,b). Results of protein analysis further revealed the presence of EV markers (e.g. CD63, CD9 and CD81) and surface markers of their donor cells (EpCAM, CD45 and CD144), respectively, in EVs (Figure S1c). All the EVs were labelled with PKH26 (red) and T-EVs were further labelled with CFSE (green) as well. Fabricated heterogeneous EVs were made by mixing T-EVs, I-EVs and E-EVs with the ratio 1:1:1. MMs modified with anti-CD45 or anti-CD144 antibodies were constructed and verified by fluorescence microscopy (Figure S2a–c) and flow cytometry analysis (Figure S2d,e). Moreover, western blot analysis suggested that CD45- and CD144-positive EVs were captured by corresponding antibody-conjugated MMs, respectively (Figure S3). Then, anti-CD45/CD144 antibody-conjugated MMs were added into the heterogeneous EVs. As shown in Figure 3b, CD45- and CD144-positive EVs were nearly completely removed from fabricated heterogeneous EVs by magnetic separation, whereas the number of T-EVs showed no obvious change (Figure 3c). As the result, the percentage of T-EVs increased significantly from 33.3% to 98.2%, thereby suggesting the high enrichment efficiency of this isolation strategy (Figure 3d). To determine whether the high enrichment efficiency of this untouched isolation strategy was reproducible for EVs of different cellular origins, other types of EVs in the fabricated heterogeneous EVs, that is I-EVs, were then employed in this study. The results revealed that I-EVs in fabricated heterogeneous EVs could also be enriched by the proposed untouched isolation strategy, suggesting the favourable universality and reliable reproducibility of our isolation strategy (Figure S4).

3.3 | Biocompatibility of the untouched isolation strategy

We next evaluated the biocompatibility of the untouched isolation strategy by comparing the characteristics of T-EVs before and after isolation. Results of TEM, NTA and DLS analysis showed no obvious difference in the morphology, size and zeta potential
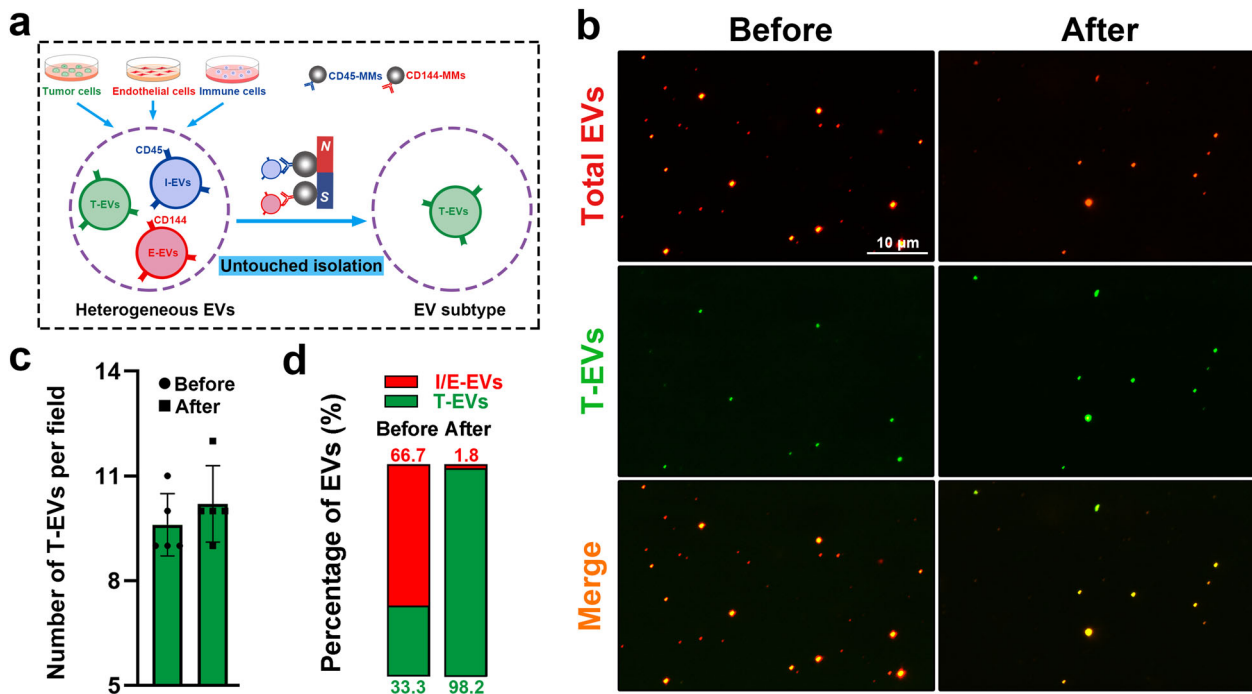
FIGURE 3 Untouched and selective enrichment of tumour-cell-derived extracellular vesicles (T-EVs). (a) Schematic diagram for untouched enrichment strategy of T-EVs. (b) Representative fluorescence images of total EVs (PKH26, red) and T-EVs (CFSE, green) before and after untouched isolation. (c) Number of T-EVs per field before and after isolation. (d) Percentages of T-EVs and non-T-EVs before and after isolation

of T-EVs before and after isolation (Figure 4a–c). The above results demonstrated that the fundamental properties of T-EVs were not affected by the untouched isolation strategy. As important intercellular communication vesicles, EVs exert their biological functions by delivering their bioactive cargoes to recipient cells. Here we tested whether the interaction between EVs and their recipient cells was affected by the untouched negative isolation strategy. Since immunomagnetic separation was currently used to separate T-EVs, here we also isolated T-EVs by EpCAM-MMs (Figure S5a–c) to make a comparison. We used confocal microscopy to display the physical interaction between EVs and HUVECs (Figure 4d). Untouched isolated T-EVs were effectively taken up by cells. However, the interaction level of EpCAM-MM-isolated T-EVs, which trapped by EpCAM-MMs on the flow of culture dish, was significantly lower than that of untouched isolated T-EVs. Results of flow cytometric analysis also confirmed that, different from positively isolated T-EVs by EpCAM-MMs, the untouched isolated T-EVs can interact with recipient cells well (Figure 4e,f). Similar results were observed in Jurkat cells (Figure S6a,b). Thus, it can be concluded that the natural properties of T-EVs, including the morphology, size, cargo composition and capability to be internalized into recipient cells, were maximally preserved by the untouched isolation strategy. The untouched isolation strategy with excellent biocompatibility would provide a method to obtain fresh T-EVs from the tumour tissues while preserving the natural properties of T-EVs.

3.4 | Untouched isolation of natural T-EVs from tumour tissues

After determining the feasibility and biocompatibility of the untouched isolation strategy, we next attempted to purify natural T-EVs from tumour tissues using this strategy. As displayed in Figure 5a, anti-CD45, anti-CD144, anti-CD41 and anti-CD235a antibody-conjugated beads were added into heterogeneous EVs from tumour tissues to capture and remove I-EVs, E-EVs, P-EVs and R-EVs. The enrichment of T-EVs from heterogeneous EVs was confirmed with confocal microscopy analysis (Figure 5b). No significant difference was detected in the number of T-EVs per field before and after isolation (Figure 5c). While, the percentage of T-EVs increased significantly from 37.5% to 92.5% (Figure 5d). Western blot analysis further indicated that the level of CD45, CD41 and CD235a in the supernatant of EVs after isolation was significantly lower than before, indicating that non-tumour-cell-derived EVs were almost removed. Whereas, there was no or only marginal difference in the level of EpCAM (Figure 5e, f). These results suggested that T-EVs in heterogeneous EVs from tumour tissues were selectively enriched by the untouched isolation strategy (Figure 5g).
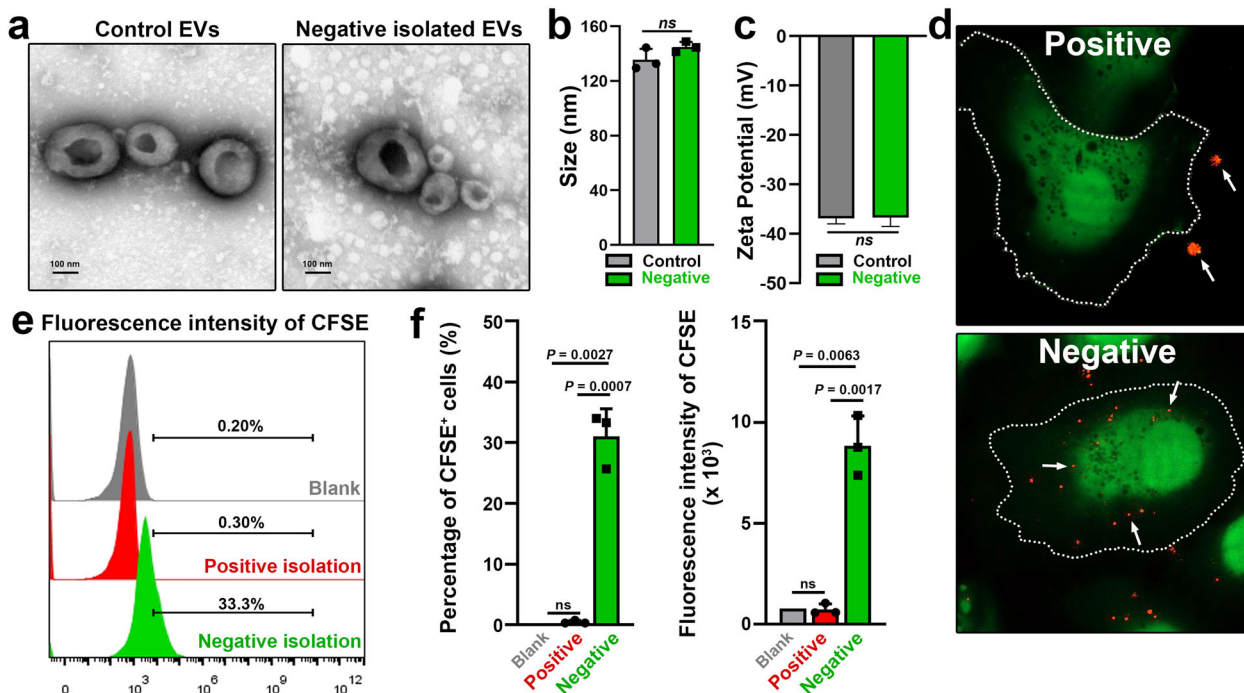
FIGURE 4 Characterization of EVs isolated by untouched (negative) isolation strategy. (a) Representative transmission electron microscopy (TEM) images of control tumour-cell-derived extracellular vesicles (T-EVs) and T-EVs gained from negative isolation strategy. Size (b) and zeta potential (c) of control T-EVs and T-EVs gained from negative isolation strategy. (d) Confocal microscopy analysis of CFSE-labelled human umbilical vein endothelial cells (HUVECs) (green) after incubation with WGA-labelled T-EVs (red) isolated by positive and negative strategy. (e) Representative histogram of HUVECs after incubation with the indicated EVs labelled with CFSE for 2 h. (f) The percentage of CFSE-positive cells and mean fluorescence intensity of CFSE in HUVECs were measured by flow cytometry

3.5 | Characterization of natural T-EVs from tumour tissues

Then, we evaluated the characteristics of tumour-tissue-derived T-EVs obtained by untouched isolation. TEM analysis revealed that natural T-EVs showed typical vesicular morphologies (Figure 6a) and their average size was 142.1 nm, which was comparable with that of heterogeneous EVs (138.7 nm) (Figure 6b, Figure S7a). There was also no significant difference in zeta potential between the purified T-EVs and heterogeneous EVs (Figure S7b). The EV markers (e.g. CD63 and CD9) in isolated T-EVs were confirmed by western blot analysis (Figure 6c). Cargo analysis was subsequently performed to gain a deeper understanding of the components carried by natural T-EVs. We revealed that tumour-associated proteins (EGFR, AKT and EpCAM) were found both in heterogeneous EVs and purified T-EVs, but their levels were significantly higher in untouched isolated T-EVs (Figure 6d), indicating distinct cargo profiles between heterogeneous EVs and T-EVs.

Angiogenesis, plays a pivotal role in cancer initiation, maintenance, progression and even immunological regulation. Growing evidence has suggested that tumour cells promote angiogenesis by secreting EVs, which can be captured by endothelial cells (Aslan et al., 2019). We then confirmed the proangiogenic role of natural T-EVs by in vitro tube formation assay using HUVECs. The results showed that, compared with heterogeneous EVs, natural T-EVs exhibited stronger proangiogenic effect, as demonstrated by the significantly increased tube formation on Matrigel (Figure 6e,f). Taken together, these results demonstrated that T-EVs were successfully purified from tumour tissues by untouched isolation without adverse effects on their integrity, cargoes and function.

3.6 | Performance of natural T-EVs from tumour tissues in vivo

To date, little study has determined the in vivo performance of natural T-EVs from tumour tissues due to technical challenges in their selective isolation. Thus, after T-EVs being successfully isolated, we fluorescently labelled T-EVs and tested there in vivo kinetics and distribution performance (Figure 7a). As shown in Figure 7b, the level of heterogeneous EVs rapidly decreased and was almost undetectable at 40 min after injection. While, the level of natural T-EVs also declined rapidly until 60 min, slightly decreased from 60 to 120 min, and eventually disappeared at 150 min after injection. These results demonstrated that the lifetime of natural T-EVs was significantly longer than heterogeneous EVs, which composed mainly of
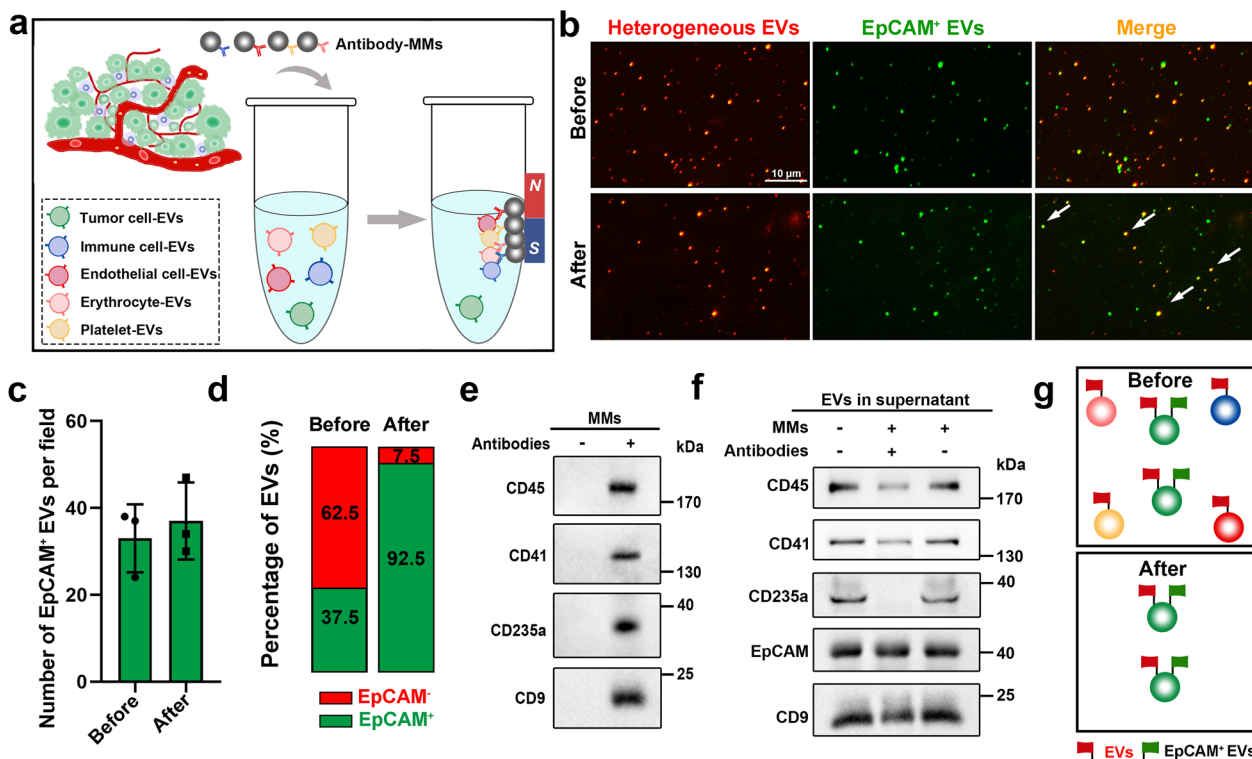
FIGURE 5 Untouched enrichment of natural tumour-cell-derived extracellular vesicles (T-EVs) from tumour tissues. (a) Schematic diagram for untouched enrichment of tumour tissue-derived T-EVs. (b) Representative fluorescence images of tumour tissue-derived heterogeneous EVs (PKH26, red) and EpCAM-positive EVs (green) before and after untouched isolation. (c) Number of EpCAM-positive EVs per field before and after the untouched isolation. (d) Percentages of EpCAM-positive and EpCAM-negative EVs before and after untouched isolation. (e) Western blot analysis of CD45, CD41, CD235a and CD9 in EVs captured on magnetic microparticles (MMs). (f) Western blot analysis of CD45, CD41, CD235a, EpCAM and CD9 in the supernatant before and after untouched isolation. (g) Schematic diagram for the enrichment of natural T-EVs by untouched isolation
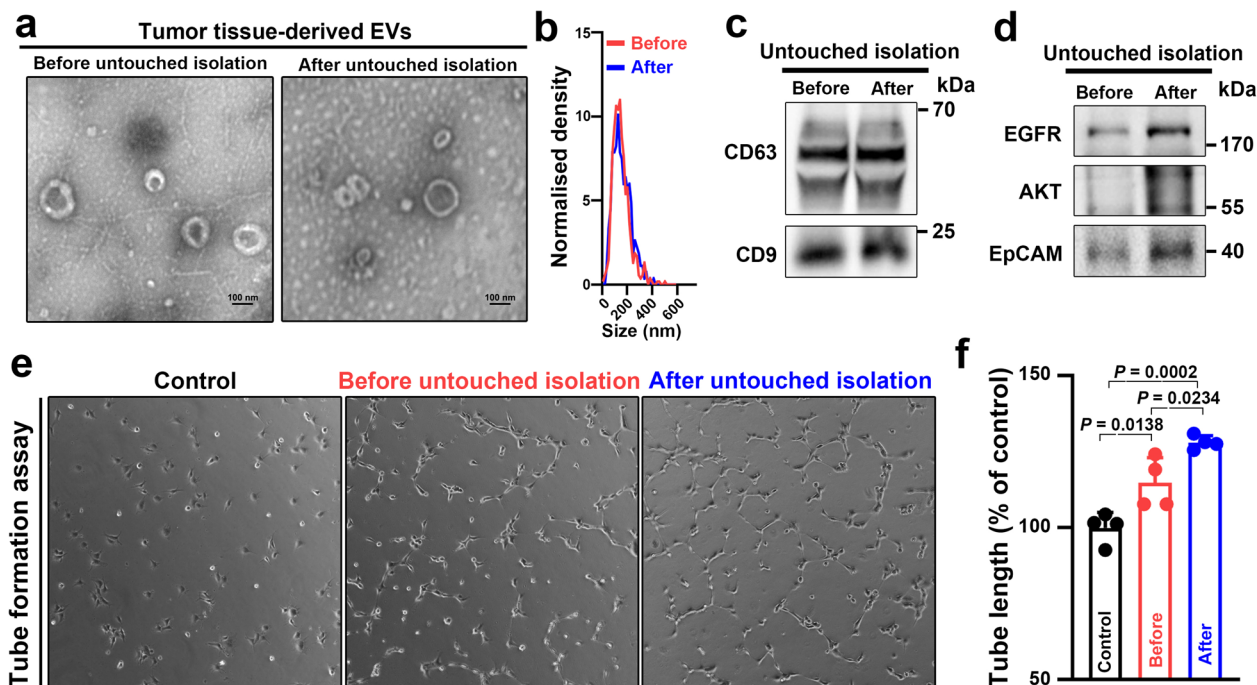

FIGURE 6 Characterization of natural tumour-cell-derived extracellular vesicles (T-EVs) isolated from tumour tissues using untouched isolation strategy. Representative transmission electron microscopy (TEM) images (a), size (b), EV markers (CD63 and CD9) (c) and tumour associated proteins (EGFR, AKT and EpCAM) (d) of tumour tissues-derived EVs before and after untouched isolation. (e, f) Proangiogenic role of heterogenous EVs (before) and natural T-EVs (after) was detected by in vitro tube formation assay
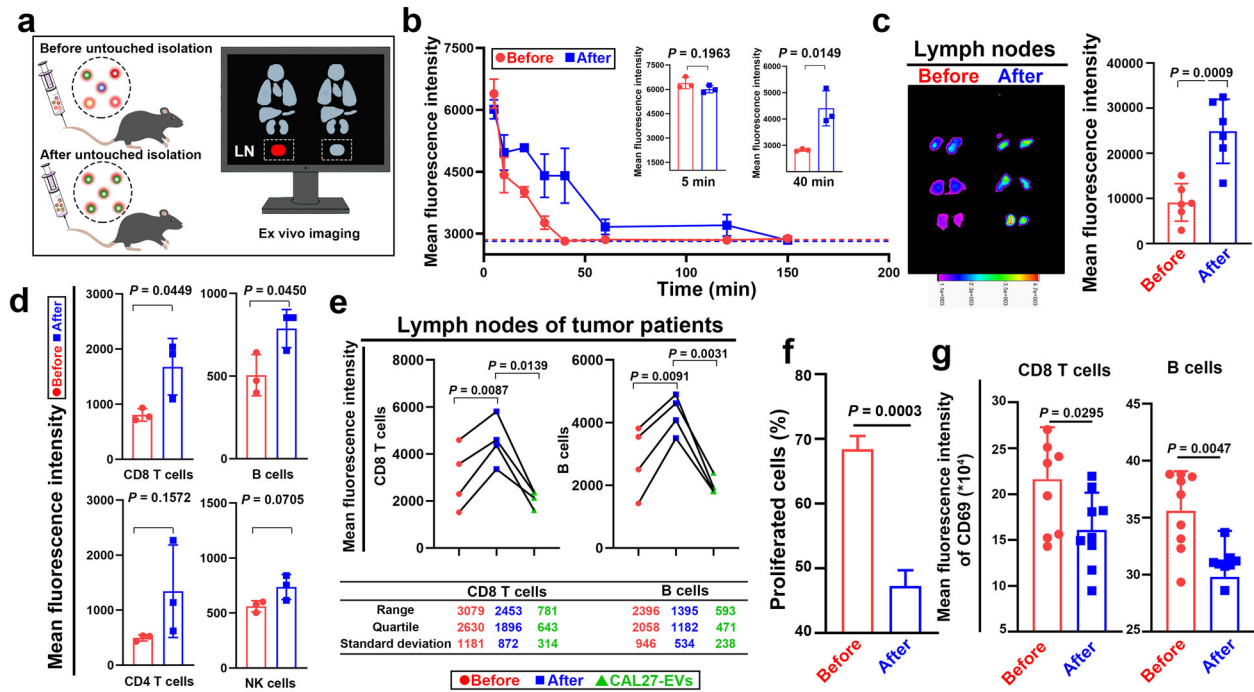
FIGURE 7 Performances of natural tumour-cell-derived extracellular vesicles (T-EVs) from OSCC patients in vivo. (a) Schematic diagram for ex vivo imaging of EVs before and after untouched isolation. (b) Levels of indicated CFSE-labelled EVs in circulation of mice after tail injection of corresponding EVs. Dashed lines represent the background signals of circulating EVs before injection of CFSE-labelled EVs. (c) Fluorescence images of lymph nodes at 12 h after tail vein injection of heterogeneous EVs and T-EVs. (d) The cellular distribution of heterogeneous EVs and T-EVs in lymph nodes of mice was determined by flow cytometry. (e) The interaction between heterogeneous EVs, T-EVs or CAL27-EVs with CD8 T cells and B cells isolated from cancer patients (top) and detailed data associated with the discrete degree analysis (bottom). (f) The proportion of human CD8 T cells and B cells with diluted CFSE dyes. (g) The level of CD69 in CD8 T cells and B cells incubated with heterogeneous EVs (before) and natural T-EVs (after)

non-tumour-cell-derived EVs. This suggests that the lifetime of T-EVs was probably longer than non-tumour-cell-derived EVs. The phagocytosis of macrophages, which is promoted by 'eat me' signal and inhibited by 'don't eat me' signal, plays a critical role in the clearance of EVs (Belhadj et al., 2020; Matsumoto et al., 2019). The results showed an increased level of the 'don't eat me' signal CD47 and a decreased level of the 'eat me' signal phosphatidylserine (PS) on T-EVs than heterogeneous EVs (Figure S8a,b), which might partially explain the longer lifetime of T-EVs than heterogeneous EVs. Then, we evaluated the signal of EVs in organs of mice. Interestingly, the signal of T-EV group in lymph nodes, but not in the brain, heart, lung, liver, kidney and spleen, was more intensive than that of heterogeneous EVs (Figures 7c and S9), indicating that T-EVs displayed enhanced lymph node-targeting specificity than non-tumour-cell-derived EVs.

Lymph nodes were composed by various immunocytes, such as T cells, B cells and natural killer (NK) cells. We then used flow cytometry analysis to further investigate the cellular distribution of EVs in lymph nodes of mice. The results showed that the level of T-EVs was significantly higher than heterogeneous EVs in CD8 T cells and B cells, whereas there was no difference or only marginal difference in CD4 T cells and NK cells (Figure 7d). Similar phenomenon was observed in immunocytes derived from OSCC patients' lymph nodes. Lymph nodes in surgical specimens of OSCC patients were harvested to prepare single-cell suspension. EVs isolated from tumour tissues were incubated with immunocytes from lymph nodes of corresponding patients. The results of flow cytometry analysis further confirmed that the interaction between natural T-EVs and CD8 T cells or B cells and the interaction level was higher than that of heterogeneous EVs (Figure 7e). Consistent with the findings by flow cytometry analysis, the results of immunofluorescence staining also showed that the signals of CFSE-labelled T-EVs in CD8 cells and B cells in lymph nodes of mice were significantly higher than that of CFSE-labelled heterogenous EVs (Figure S10). These results suggest that natural T-EVs may play immunomodulatory effects through CD8 T cells and B cells.

Currently, EVs separated from in vitro cultured tumour cell lines were widely employed to investigate the performance of T-EVs. We here compared the interaction of natural T-EVs from tissues of OSCC patients and OSCC cell line (CAL27 cell)-derived EVs (CAL27-EVs) with CD8 T cells or B cells. As shown in Figure 7e, the interaction of CAL27-EVs with CD8 T cells and B cells was significantly lower that of natural T-EVs. This result indicates that cell-line-derived EVs may have different performances in comparison to the natural T-EVs secreted in vivo. Furthermore, we also found that the range, quartile and standard deviation of the data in CAL27-EVs group were significantly lower than T-EVs isolated from different cancer patients (Figure 7e).

Then, we further evaluated the effects of T-EVs on CD8 T cells and B cells. T-EVs and heterogeneous EVs isolated from tumour tissues were cocultured with lymph node cells isolated from the corresponding patients. The results revealed that both

heterogeneous EVs and natural T-EVs inhibited the proliferation and activation of CD8 T cells and B cells, as demonstrated by decreased proportion of cells containing diluted CFSE, and reduced expression of CD69 (Figure 7f,g). While, compared with heterogeneous EVs, natural T-EVs, carrying higher levels of tumour-associated bioactive molecules, showed increased immunosuppressive effects on CD8 T cells and B cells.

4 | DISCUSSION

In the past decade, the number of EV-related studies have experienced a blowout. However, with the gradual deepening of the studies, challenges and problems regarding the further understanding and application of EVs have begun to emerge. Studies demonstrated that the size and composition of EVs are heterogeneous and largely based on their cellular sources and biological environment of parent cells. The EVs in tumour tissues are released from tumour cells and non-tumour cells. Therefore, to identify their fundamental characteristics and biological functions more accurately, the first and essential step is to separate T-EVs from non-tumour-cell-derived EVs. However, the conventional isolation methods including ultracentrifugation and precipitation are based on EVs' physical properties (density or solubility) and thereby are incapable of separating EV subpopulations. In the past few years, some isolating techniques, including microfluidic-based isolation, have been newly developed to isolate EV subpopulations with different size, electrical characteristics and deformability. EV subpopulations with certain surface markers can be successfully captured and isolated via immunoaffinity-based separation. However, such strategies are dependent on immunoaffinity, which involves the binding and dissociation between surface markers of EVs and antibodies immobilized on the narrow channels of microfluidic chips, and will compromise the natural properties and functions of EVs. Thus, selective purification strategies of T-EVs, which could maximally preserve their natural properties and functions, are highly needed.

Inspired by our years of experience in the isolation of EVs, we here designed an untouched isolation strategy to isolate T-EVs from tumour tissues without unfavourable effects on their natural properties for the first time. In brief, T-EVs were enriched by removing the undesired non-tumour-cell-derived EVs with antibody-conjugated MMs. We determined their fundamental characteristics and cargo composition, and revealed the in vivo biological behaviours, especially their distribution pattern and kinetic characteristics. The observed difference in the lifetime of EVs would be closely related to their distinct surface proteins. Our recent study has reported that circulating EVs with different cell sources carry different surface proteins and have distinct lifetimes (Yu et al., 2021). Moreover, previous studies have also demonstrated that macrophage-mediated phagocytosis, regulated by the 'eat me' and 'don't eat me' signals, plays an important role in the clearance of EVs from the circulation. CD47, being known as a 'don't eat me' signal, is usually overexpressed on the surface of many types of tumour cells and can inhibit the phagocytosis of tumour cells by macrophages. T-EVs may evade the phagocytosis of macrophages by inheriting surface CD47 from their donor cells, resulting in the longer lifetime of tumour cell-derived EVs. Additionally, PS is an essential component in all human cells, which is present on the inner leaflet of the cell membrane. Once exposed on the surface of cells, mainly apoptotic cells, it would serve as an 'eat me' signal to the phagocytes and result in engulfment. We here revealed the increased level of 'don't eat me' signal CD47 and decreased level of 'eat me' signal PS on T-EVs than heterogeneous EVs (Figure S8), providing possible reasons for the longer lifetime of T-EVs.

Moreover, we found that T-EVs exhibited a higher immunosuppression effect on CD8 T cells and B cells in lymph nodes than heterogeneous EVs. According to the previous studies, several reasons may account for the enhanced immunoinhibitory effect of purified T-EVs. First, T-EVs, which exhibited powerful immunoinhibitory effects in various reports, were selectively enriched after untouched isolation. This means increased level of T-EVs in the same amount of EVs. Second, recent study reported that immunocyte-derived EVs attenuates immunoinhibitory effect induced by T-EVs (Qiu et al., 2021). Once the non-tumour-cell-derived EVs, especially the immunocyte-derived EVs, were removed by negative sorting strategy, the immunoinhibitory effect of T-EVs may be further revealed. However, more mechanisms involved in the immunosuppressive effect of purified T-EVs require further studies. Taken together, our data also suggest that, due to the different profiles of cargoes, T-EVs and non-tumour-cell-derived EVs may have distinct performance. Therefore, T-EVs should be selectively isolated from tumour tissues for an accurate evaluation of their behaviours and functions.

Due to the availability, in vitro cultured tumour-cell-line-derived EVs are currently used to study the roles of T-EVs in tumour initiation and progression. Using those cell culture-derived EVs, previous studies have reported that T-EVs play a critical role in immunosuppression and tumour angiogenesis. In present study, we revealed the enhanced immunosuppressive effect of natural T-EVs from tissues when compared with tumour-cell-line-derived EVs. More importantly, we found that the range, quartile and standard deviation of the data in tumour-cell-line-derived EVs were significantly lower than T-EVs isolated from different cancer patients (Figure 7e). Indeed, due to the heterogeneous tumour microenvironment and tumour stage among patients, T-EVs released by different patients may have different performances. Whereas, the heterogeneity in their performances was concealed by using tumour-cell-line-derived EVs. Therefore, the performance of cell-line-derived EVs cannot represent the real properties of natural T-EVs. This reminds us that tumour-tissue-derived T-EVs can more accurately reflect the pathophysiological characteristics and behaviours of real T-EVs, and are the better source for accurate functional analysis.

In summary, we developed the first untouched isolation strategy to specifically isolate T-EVs from tumour tissues without unfavourable effects on their natural properties. T-EVs were enriched by removing the undesired EVs. Since the isolating materials were directly binding to the undesired non-tumour-cell-derived EVs rather than the desired T-EVs, the natural biological properties and cargo composition of T-EVs were not affected during the isolation. Using the proposed isolation method, we successfully purified natural T-EVs from the tumour tissues of cancer patients and revealed their distribution pattern and kinetics characteristics for the first time. Moreover, tumour-tissue-derived T-EVs exhibited a higher immunosuppression effect on CD8 T cells and B cells in lymph nodes than non-tumour cell-derived EVs. Moreover, results revealed that tumour tissue-derived T-EVs can more accurately reflect the pathophysiological characteristics and behaviours of real T-EVs than tumour-cell-line-derived EVs. Taken together, by providing the first reliable untouched isolation strategy for selective isolation of T-EVs from patients, our present work takes an extraordinary step forward in the isolation of EV subpopulation. It can also be expected that the combination between untouched isolation strategy and microfluidic chips would dramatically accelerate the investigation of heterogeneity of EVs in cellular origin.

CONFLICT OF INTEREST

All authors declare no potential conflict of interest.

AUTHOR CONTRIBUTIONS

Conceptualization: Zi-Li Yu, Xing-Chi Liu, Min Wu, Shan Shi, Qiu-Yun Fu, Jun Jia, Gang Chen and Gang Chen. *Data curation*: Zi-Li Yu, Xing-Chi Liu, Min Wu, Shan Shi, Qiu-Yun Fu, Jun Jia and Gang Chen. *Formal analysis*: Zi-Li Yu, Xing-Chi Liu, Min Wu, Shan Shi, Qiu-Yun Fu, Jun Jia and Gang Chen. *Funding acquisition*: Zi-Li Yu, Xing-Chi Liu, Min Wu, Shan Shi, Qiu-Yun Fu, Jun Jia and Gang Chen. *Investigation*: Zi-Li Yu, Xing-Chi Liu, Min Wu, Shan Shi, Qiu-Yun Fu, Jun Jia and Gang Chen. *Methodology*: Zi-Li Yu, Xing-Chi Liu, Min Wu, Shan Shi, Qiu-Yun Fu, Jun Jia and Gang Chen. *Project administration*: Zi-Li Yu, Xing-Chi Liu, Min Wu, Shan Shi, Qiu-Yun Fu, Jun Jia and Gang Chen. *Resources*: Zi-Li Yu, Xing-Chi Liu, Min Wu, Shan Shi, Qiu-Yun Fu, Jun Jia and Gang Chen. *Software*: Zi-Li Yu, Xing-Chi Liu, Min Wu, Qiu-Yun Fu, Jun Jia and Gang Chen. *Supervision*: Zi-Li Yu, Xing-Chi Liu, Min Wu, Shan Shi, Qiu-Yun Fu, Jun Jia and Gang Chen. *Validation*: Zi-Li Yu, Xing-Chi Liu, Min Wu, Shan Shi, Qiu-Yun Fu, Jun Jia and Gang Chen. *Visualization*: Zi-Li Yu, Xing-Chi Liu, Shan Shi, Qiu-Yun Fu, Jun Jia and Gang Chen. *Writing – original draft*: Zi-Li Yu, Xing-Chi Liu, Min Wu, Shan Shi, Qiu-Yun Fu, Jun Jia and Gang Chen. *Writing – review & editing*: Zi-Li Yu, Xing-Chi Liu, Min Wu, Shan Shi, Qiu-Yun Fu, Jun Jia and Gang Chen.

ORCID

Zi-Li Yu https://orcid.org/0000-0003-0728-8564
Jun Jia https://orcid.org/0000-0002-9593-5567
Gang Chen https://orcid.org/0000-0003-3332-3511

REFERENCES

Aslan, C., Maralbashi, S., Salari, F., Kahroba, H., Sigaroodi, F., Kazemi, T., & Kharaziha, P. (2019). Tumor-derived exosomes: Implication in angiogenesis and antiangiogenesis cancer therapy. *Journal of Cellular Physiology*, *234*(10), 16885–16903. [CrossRef] PMID: 30793767.

Belhadj, Z., He, B., Deng, H., Song, S., Zhang, H., Wang, X., Dai, W., & Zhang, Q. (2020). A combined "eat me/don't eat me" strategy based on extracellular vesicles for anticancer nanomedicine. *Journal of Extracellular Vesicles*, *9*(1), 1806444. [CrossRef] PMID: 32944191.

Cai, S., Luo, B., Jiang, P., Zhou, X., Lan, F., Yi, Q., & Wu, Y. (2018). Immuno-modified superparamagnetic nanoparticles via host-guest interactions for high-purity capture and mild release of exosomes. *Nanoscale*, *10*(29), 14280–14289. [CrossRef] PMID: 30014056.

Casadei, L., Choudhury, A., Sarchet, P., Mohana Sundaram, P., Lopez, G., Braggio, D., Balakirsky, G., Pollock, R., & Prakash, S. (2021). Cross-flow microfiltration for isolation, selective capture and release of liposarcoma extracellular vesicles. *Journal of Extracellular Vesicles*, *10*(4), E12062. [CrossRef] PMID: 33643547.

Chen, G., Huang, A. C., Zhang, W., Zhang, G., Wu, M., Xu, W., Yu, Z., Yang, J., Wang, B., Sun, H., Xia, H., Man, Q., Zhong, W., Antelo, L. F., Wu, B., Xiong, X., Liu, X., Guan, L., Li, T., & Guo, W. (2018). Exosomal PD-L1 contributes to immunosuppression and is associated with anti-PD-1 response. *Nature*, *560*(7718), 382–386. [CrossRef] PMID: 30089911.

Chen, G., Zhu, J.-Y., Zhang, Z.-L., Zhang, W., Ren, J.-G., Wu, M., Hong, Z.-Y., Lv, C., Pang, D.-W., & Zhao, Y.-F. (2015). Transformation of cell-derived microparticles into quantum-dot-labeled nanovectors for antitumor siRNA delivery. *Angewandte Chemie (International ed in English)*, *54*(3), 1036–1040. [CrossRef] PMID: 25412570.

Crescitelli, R., LäSser, C., & LöTvall, J. (2021). Isolation and characterization of extracellular vesicle subpopulations from tissues. *Nature Protocols*, *16*(3), 1548–1580. [CrossRef] PMID: 33495626.

Domcke, S., Sinha, R., Levine, D. A., Sander, C., & Schultz, N. (2013). Evaluating cell lines as tumour models by comparison of genomic profiles. *Nature Communication*, 4, 2126. [CrossRef] PMID: 23839242.

Hoshino, A., Costa-Silva, B., Shen, T.-L., Rodrigues, G., Hashimoto, A., Tesic Mark, M., Molina, H., Kohsaka, S., Di Giannatale, A., Ceder, S., Singh, S., Williams, C., Soplop, N., Uryu, K., Pharmer, L., King, T., Bojmar, L., Davies, A. E., Ararso, Y., & Lyden, D. (2015). Tumour exosome integrins determine organotropic metastasis. *Nature*, 527(7578), 329–335. [CrossRef] PMID: 26524530.

Jeppesen, D. K., Fenix, A. M., Franklin, J. L., Higginbotham, J. N., Zhang, Q., Zimmerman, L. J., Liebler, D. C., Ping, J., Liu, Q., Evans, R., Fissell, W. H., Patton, J. G., Rome, L. H., Burnette, D. T., & Coffey, R. J. (2019). Reassessment of exosome composition. *Cell*, 177(2), 428–445.e18. [CrossRef] PMID: 30951670.

Kalluri, R., & Lebleu, V. S. (2020). The biology, function, and biomedical applications of exosomes. *Science*, 367(6478), Eaau6977. [CrossRef] PMID: 32029601.

Liu, C., Xu, X., Li, B., Situ, B., Pan, W., Hu, Y., An, T., Yao, S., & Zheng, L. (2018). Single-exosome-counting immunoassays for cancer diagnostics. *Nano Letters*, 18(7), 4226–4232. [CrossRef] PMID: 29888919.

Liu, C., Zhao, J., Tian, F., Chang, J., Zhang, W., & Sun, J. (2019). λ-DNA- and aptamer-mediated sorting and analysis of extracellular vesicles. *Journal of the American Chemical Society*, 141(9), 3817–3821. [CrossRef] PMID: 30789261.

Matsumoto, A., Takahashi, Y., Chang, H.-Y., Wu, Y.-W., Yamamoto, A., Ishihama, Y., & Takakura, Y. (2019). Blood concentrations of small extracellular vesicles are determined by a balance between abundant secretion and rapid clearance. *Journal of Extracellular Vesicles*, 9(1), 1696517. [CrossRef] PMID: 31807238.

Möller, A., & Lobb, R. J. (2020). The evolving translational potential of small extracellular vesicles in cancer. *Nature Reviews Cancer*, 20(12), 697–709. [CrossRef] PMID: 32958932.

Morrissey, S. M., Zhang, F., Ding, C., Montoya-Durango, D. E., Hu, X., Yang, C., Wang, Z., Yuan, F., Fox, M., Zhang, H.-G., Guo, H., Tieri, D., Kong, M., Watson, C. T., Mitchell, R. A., Zhang, X., Mcmasters, K. M., Huang, J., & Yan, J. (2021). Tumor-derived exosomes drive immunosuppressive macrophages in a pre-metastatic niche through glycolytic dominant metabolic reprogramming. *Cell Metabolism*, 33(10), 2040–2058.e10. [CrossRef] PMID: 34559989.

Qiu, Y., Yang, Y., Yang, R., Liu, C., Hsu, J.-M., Jiang, Z., Sun, L., Wei, Y., Li, C.-W., Yu, D., Zhang, J., & Hung, M.-C. (2021). Activated T cell-derived exosomal PD-1 attenuates PD-L1-induced immune dysfunction in triple-negative breast cancer. *Oncogene*, 40(31), 4992–5001. [CrossRef] PMID: 34172932.

Ramirez, M. I., Amorim, M. G., Gadelha, C., Milic, I., Welsh, J. A., Freitas, V. M., Nawaz, M., Akbar, N., Couch, Y., Makin, L., Cooke, F., Vettore, A. L., Batista, P. X., Freezor, R., Pezuk, J. A., Rosa-Fernandes, L., Carreira, A. C. O., Devitt, A., Jacobs, L., & Dias-Neto, E. (2018). Technical challenges of working with extracellular vesicles. *Nanoscale*, 10(3), 881–906. [CrossRef] PMID: 29265147.

Raposo, G., & Stoorvogel, W. (2013). Extracellular vesicles: Exosomes, microvesicles, and friends. *Journal of Cell Biology*, 200(4), 373–383. [CrossRef] PMID: 23420871.

Reátegui, E., Van Der Vos, K. E., Lai, C. P., Zeinali, M., Atai, N. A., Aldikacti, B., Floyd, F. P. H., Khankhel, A., Thapar, V., Hochberg, F. H., Sequist, L. V., Nahed, B. V. S., Carter, B., Toner, M., Balaj, L., Ting, T. D., Breakefield, X. O., & Stott, S. L. (2018). Engineered nanointerfaces for microfluidic isolation and molecular profiling of tumor-specific extracellular vesicles. *Nature Communication*, 9(1), 175. [CrossRef] PMID: 29330365.

Ren, J. G., Man, Q. W., Zhang, W., Li, C., Xiong, X. P., Zhu, J. Y., Wang, W. M., Sun, Z. J., Jia, J., Zhang, W. F., Zhao, Y. F., Chen, G., & Liu, B. (2016a). Elevated level of circulating platelet-derived microparticles in oral cancer. *Journal of Dental Research*, 95(1), 87–93. [CrossRef] PMID: 26124218.

Ren, J. G., Zhang, W., Liu, B., Man, Q. W., Xiong, X. P., Li, C., Zhu, J. Y., Wang, W. M., Jia, J., Sun, Z. J., Zhang, W. F., Chen, G., & Zhao, Y. F. (2016b). Clinical significance and roles in angiogenesis of circulating microparticles in oral cancer. *Journal of Dental Research*, 95(8), 860–867. [CrossRef] PMID: 27013642.

Shao, H., Im, H., Castro, C. M., Breakefield, X., Weissleder, R., & Lee, H. (2018). New technologies for analysis of extracellular vesicles. *Chemical Reviews*, 118(4), 1917–1950. [CrossRef] PMID: 29384376.

Sharma, P., Ludwig, S., Muller, L., Hong, C. S., Kirkwood, J. M., Ferrone, S., & Whiteside, T. L. (2018). Immunoaffinity-based isolation of melanoma cell-derived exosomes from plasma of patients with melanoma. *Journal of Extracellular Vesicles*, 7(1), 1435138. [CrossRef] PMID: 29511460.

Tkach, M., & Théry, C. (2016). Communication by extracellular vesicles: Where we are and where we need to go. *Cell*, 164(6), 1226–1232. [CrossRef] PMID: 26967288.

Veerman, K., Tardiveau, C., & Martins, F., et al. (2019). Single-cell analysis reveals heterogeneity of high endothelial venules and different regulation of genes controlling lymphocyte entry to lymph nodes. *Cell Reports*, 26(11), 3116–3131.e5.

Wang, J., Ma, P., Kim, D. H., Liu, Bi-F., & Demirci, U. (2021). Towards microfluidic-based exosome isolation and detection for tumor therapy. *Nano Today*, 37, 101066. [CrossRef] PMID: 33777166.

Welsh, J. A., Van Der Pol, E., Arkesteijn, G. J. A., Bremer, M., Brisson, A., Coumans, F., Dignat-George, F., Duggan, E., Ghiran, I., Giebel, B., Görgens, A., Hendrix, A., Lacroix, R., Lannigan, J., Libregts, S. F. W. M., Lozano-Andrés, E., Morales-Kastresana, A., Robert, S., De Rond, L., & Jones, J. C. (2020). MIFlowCyt-EV: A framework for standardized reporting of extracellular vesicle flow cytometry experiments. *Journal of Extracellular Vesicles*, 9(1), 1713526. [CrossRef] PMID: 32128070.

Xu, R., Rai, A., Chen, M., Suwakulsiri, W., Greening, D. W., & Simpson, R. J. (2018). Extracellular vesicles in cancer implications for future improvements in cancer care. *Nature Reviews Clinical Oncology*, 15(10), 617–638. [CrossRef] PMID: 29795272.

Yu, Z.-L., Zhao, Y., Miao, F., Wu, M., Xia, H.-F., Chen, Z.-K., Liu, H.-M., Zhao, Y.-F., & Chen, G. (2021). In situ membrane biotinylation enables the direct labeling and accurate kinetic analysis of small extracellular vesicles in circulation. *Analytical Chemistry*, 93(31), 10862–10870. [CrossRef] PMID: 34328732.

Zhang, W., Yu, Z.-L., Wu, M., Ren, J.-G., Xia, H.-F., Sa, G.-L., Zhu, J.-Y., Pang, D.-W., Zhao, Y.-F., & Chen, G. (2017). Magnetic and folate functionalization enables rapid isolation and enhanced tumor-targeting of cell-derived microvesicles. *ACS Nano*, 11(1), 277–290. [CrossRef] PMID: 28005331.

Zhong, W.-Q., Ren, J.-G., Xiong, X.-P., Man, Q.-W., Zhang, W., Gao, L., Li, C., Liu, B., Sun, Z.-J., Jia, J., Zhang, W.-F., Zhao, Y.-F., & Chen, G. (2019). Increased salivary microvesicles are associated with the prognosis of patients with oral squamous cell carcinoma. *Journal of Cellular and Molecular Medicine*, 23(6), 4054–4062. [CrossRef] PMID: 30907490.

SUPPORTING INFORMATION

Additional supporting information may be found in the online version of the article at the publisher's website.